Proceedings of the 2nd Biennial IEEE/RAS-EMBS International Conference on Biomedical Robotics and Biomechatronics Scottsdale, AZ, USA, October 19-22, 2008

Force Control of a Permanent Magnet for Minimally-Invasive Procedures

Reuben D. Brewer[1], Kevin E. Loewke[1], Eugene F. Duval[3], and J. Kenneth Salisbury[1,2]
[1]Department of Mechanical Engineering, Stanford University, Stanford, CA
[2]Departments of Computer Science and Surgery, Stanford University, Stanford, CA
[3]Duval Design, Menlo Park, CA
rdbrewer@stanford.edu, kloewke@stanford.edu, EDuval1047@aol.com, jks@robotics.stanford.edu

***Abstract*— Magnetic actuation can be used for minimally invasive control of medical devices such as robotic catheters. However, current systems that use large permanent magnets are limited in their ability to modulate the magnetic force. In this paper we present a proof-of-concept system for closed-loop force control of a permanent magnet using shielding materials. Our system consists of a device that actuates pieces of high-permeability metal to redirect magnetic lines of flux. This is used to regulate the attractive force exerted by a large controlling magnet on a smaller moving magnet. We compare the performance of our system to FEA simulations and present experimental results for constant-force control at forces and distances that are medically relevant.**

I. INTRODUCTION

The growing popularity of minimally invasive robotic surgery has led to the development of many new and increasingly complex systems [13], [9], [16]. The actuation and control of these systems depend on the type of instruments being used as well as the targeted anatomical locations. For example, systems designed for laparoscopic or "keyhole" surgery employ sensors and actuators on well-defined linkages and tools [11]. However, for systems that use flexible or compliant instruments, such as robotic catheters, placement of these sensors and actuators is not as well defined. This is particularly the case since most catheters are designed to navigate to hard-to-reach anatomical locations through small and tortuous paths. Current methods for actuating robotic catheters include the use of pull wires embedded within a compliant tube [8], [3] as well as super-elastic backbones [19].

Another technique for controlling robotic catheters in a minimally invasive manner is magnetic actuation. The general idea is that the catheter can be equipped with small magnets at the distal tip, while a much larger magnet located outside of the body provides a controlling force and/or torque. The concept of magnetic actuation dates back to 1951 for manipulating a catheter to the aorta [17]. Since then, the introduction of robotics and computer-aided systems has led to the development of more sophisticated techniques. One of the first commercial products, developed by Stereotaxis, Inc. [5], used 3 orthogonal electromagnets cooled by liquid helium to control a magnetic catheter [10], [18]. The 3 electromagnets in their system were subsequently replaced by 2 large rare-earth permanent magnets with positioners for rotation and translation [14]. This system creates a spherical volume with 20-cm diameter of constant magnetic force and variable orientation. The magnetic field regulates the orientation of the catheter tip by rotating the large magnets, while the proximal end of the catheter is advanced using a feeder mechanism.

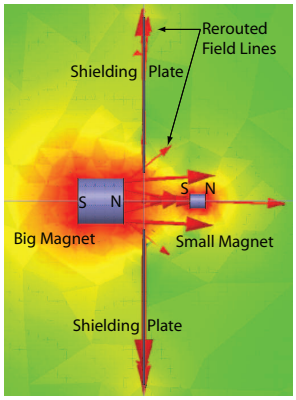

Fig. 1. FEA simulation of our experimental setup, showing how inserting a magnetic shielding material between two magnets reroutes field lines through the shielding material, reducing the force on the small magnet. Darker color denotes higher magnetic flux density.

One of the limitations of the permanent magnet system in [14] is that it lacks the ability to provide variable force. Attempting to modulate the magnetic force with reasonable bandwidth by moving these magnets would be very difficult due to their large size and inertia. In many applications, however, the physician may need to vary the amount of force they exert on the catheter depending on the anatomy and type of procedure. One solution is to use large electromagnets as demonstrated in [10], but the size and cost of such a system may be prohibitive. An alternative solution that has not been explored for medical applications is to modulate the magnetic force by placing controllable shielding materials between the large and small magnets. The magnetic shield works by using highly permeable material to redirect magnetic lines of flux [15] through itself and away from the small magnet. When controlled electromechanically, the shielding material can be actuated to provide force control at a reasonable bandwidth. For medical applications, the ability to modulate the magnetic force allows for smaller external magnets that

978-1-4244-2883-0/08/$25.00 ©2008 IEEE

can be brought in closer to the patient, as opposed to larger magnets that must be kept sufficiently far away to create a working space of constant force.

In this paper we present a proof-of-concept system for closed-loop control of magnetic force using shielding materials. Our setup, as shown in Figure 1, uses two plates of high permeability shielding material called Hymu-80 [6] that are oriented perpendicular to the large magnetic field. The shielding plates are attached to a spreading mechanism that opens and closes the plates to vary the amount of force exerted on the small magnet. This small magnet could in principle be attached to a catheter, endoscopic capsule [2], or other medical device. This benchtop system is designed to control force in one direction only, although the concept can be extended to accommodate additional degrees-of-freedom.

In the following sections we begin with a theoretical background on magnetic shielding. We then demonstrate a simple usage of magnetic shielding for force control of a permanent magnet and compare this to software simulations. Next we present the mechanical design of our force control system and describe a control strategy using successive loop closure. Finally, we present experimental data from proof-of-concept operation and address future work.

II. MAGNETIC FORCE CONTROL USING SHIELDING

We can reduce the force between two magnets by inserting a highly-permeable magnetic shielding material between the magnets. The magnetic shielding reroutes the field lines between the magnets through the shielding itself, thereby reducing the magnetic flux that one magnet exerts on the other [12]. An FEA simulation of this effect is shown in Figure 1. The magnetic force F is proportional to the gradient of the magnetic flux B:

$$F = m\nabla B. \tag{1}$$

Note that m is simply the magnetic dipole moment of the magnet and is an inherent property. By rerouting the flux lines that the magnets exert on each other, the shielding material reduces the gradient of the flux density at each magnet and, therefore, the force between the magnets.

A. Selection of Shielding and Magnets

The magnetic shielding is able to reroute the field lines because field lines follow the path of highest magnetic permeability, much as current flows through the path of highest electrical conductance. Magnetic permeability is an inherent material property that describes how easily an externally applied magnetic field induces magnetic flux in the material, or reroutes the field lines. Similarly, magnetic saturation describes the material's maximum ability to route field lines, or the maximum flux that can be induced. The ideal shielding setup is to use a material that has high permeability to attract the field lines as well as a high saturation to reroute a large amount of flux. However, it is difficult to find materials with both desirable properties. After looking at several options, as shown in Table 1, we selected Hymu-80 due to its relative low cost and high permeability.

TABLE I
COMPARISON OF SHIELDING MATERIAL PROPERTIES

Material	Max. Permeability	Saturation(KGauss)
Hyperco-50 [4]	10,000	24
Nickel-50 [7]	80,000	15.5
Hymu-80 [6]	325,000	8

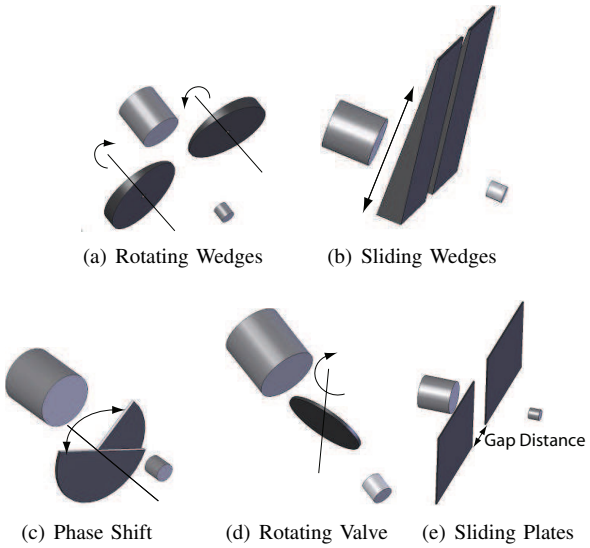

(a) Rotating Wedges (b) Sliding Wedges

(c) Phase Shift (d) Rotating Valve (e) Sliding Plates

Fig. 2. Different shielding geometries for reducing the magnetic force on the small magnet.

By controlling the quantity and location of magnetic shielding between two magnets, we can control how much of a force reduction occurs between the magnets. Figure 2 shows several potential geometries that could be actuated toward this end. The wedge designs would use linear or rotary motion to control the thickness of shielding material nearest to the common axis of the magnets. The rotating valve design would rotate the shielding material to change the projected area that faces the poles of the magnets. The phase shift/PWM design would control the arc length of the gap in shielding and could possibly be spun rapidly to produce a force drive similar to pulse-width modulation (PWM). However, a potential detraction of all of the above designs is that they involve some degree of asymmetrical shielding that could rotate the small magnet and pull it in a direction misaligned with the axis of the big magnet. A simpler, symmetrical design is the sliding plates configuration, wherein two shielding plates constrained to move only in-plane would use an adjustable gap between them to control the force reduction. For simplicity of design and analysis, we selected the sliding plates configuration for our proof-of-concept device. We chose a plate thickness of 1/16" since it was the most convenient to machine.

We used neodymium rare-earth magnets for their high magnetic field strength. The controlling magnet was a N42 Grade cylindrical magnet magnetized along its axis with a diameter and length of 38.1mm. The small magnet was the

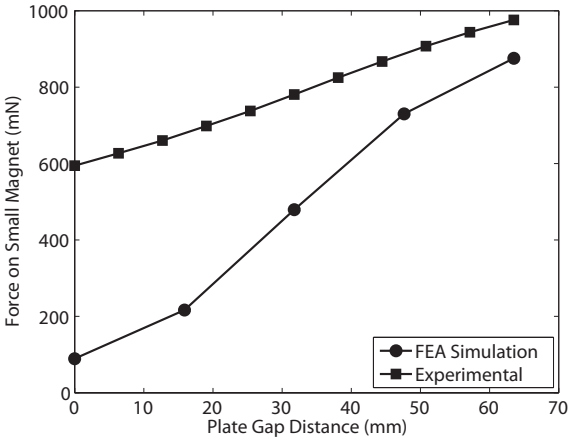

Fig. 3. Comparison of simulated and experimental forces on the small magnet.

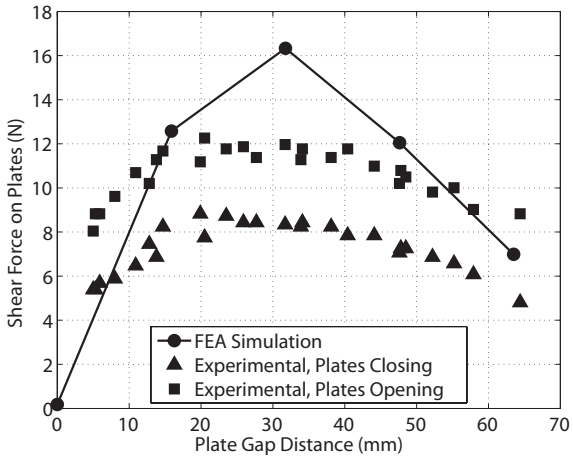

Fig. 4. Comparison of simulated and experimental forces on the shielding plates as a function of plate gap distance. Note that the shear force always works to close the plates.

same grade as the controlling magnet but with a diameter and length of 12.7mm. These magnet sizes provided forces and a workspace approaching what would be necessary for a practical medical system.

B. Shielding, Magnetic Force Relationship

Having selected the plate design, we used a magnetic finite element analysis (FEA) package, Maxwell 3D [1], to predict the forces on the small magnet as well as on the shielding plates in their sliding direction. The variable of interest was the in-plane gap distance between the shielding plates. The controlling magnet was placed at a distance of 16.5mm from the shielding plates, and the small magnet was placed at a distance of 38.1mm from the shielding plates on the opposite side.

As shown in Figure 3, the simulation predicts a roughly linear relationship between plate gap distance and force on the small magnet over a workspace of 65mm, with slight flattening at either end of the workspace. As shown in Figure 4, the simulation predicts a parabolic relationship between plate gap distance and in-plane shear force that always works to close the plates, with the maximum force acting in the middle of the workspace.

Experimental measurements of these force relationships are shown in Figures 3 and 4 and confirm the predictions of roughly linear and parabolic profiles, respectively. However, the experimental measurements differ somewhat in their magnitude from the simulations. In both cases, it appears that the shielding plates are unable to shield as efficiently as predicted. With respect to force on the small magnet, the predicted and experimental forces are comparable at the maximum gap distance where the plates are quite far from the magnets and exert little influence, but the predicted minimum force is much lower than was obtained experimentally. This suggests that the plates are not rerouting as many field lines away from the small magnet as expected. With respect to the shear force on the plates, the maximum predicted force is higher than was obtained experimentally, again suggesting that the plates are not rerouting enough field lines to exert the higher predicted shear force. Another interesting difference is the significant hysteresis in the shear force that appears from measuring the shear force when the plates were opening and closing. The fact that the magnitude of the hysteresis is much larger than the friction in the sliding mechanism suggests that the hysteresis is due to the magnetic force. A natural explanation for the reduced experimental shielding capacity is the saturation limit that was discussed previously, but this requires further investigation.

III. MECHANICAL DESIGN

To obtain higher shielding capacity than we observed experimentally in the above initial setup, our final mechanical system, as shown in Figure 5, doubled the thickness of the shielding plates by stacking pairs of the 1/16" plates. Figures 6 and 7 show roughly linear small magnet force and parabolic shear force profiles, respectively, that are similar to those predicted for the single plate setup. Note, however, that the region of linearity for the small magnet force is over a reduced workspace, with increased flattening on the ends.

The mechanical system for actuating the shielding plates consists of a plate-spreader mechanism to control the gap distance between the plates, a counterbalance system to cancel the magnetic shear force on the plates, and a weighing setup to measure the force on the small magnet indirectly.

A. Plate-spreader

The plate-spreader uses a Maxon RE-30 DC motor that is connected remotely via belt to a rack and pinion system at the plates. Each plate has a rack mounted on it and is constrained to 1-D translation via two miniature linear slides beneath it. Rotating the motor separates the plates symmetrically about the large magnet. To prevent unintended magnetic interaction, we placed the motor far away from the large magnet and used magnetic materials as minimally as possible in the overall structure. The use of two linear slides introduced some friction from imperfect parallel alignment but was deemed necessary since the the single linear slides

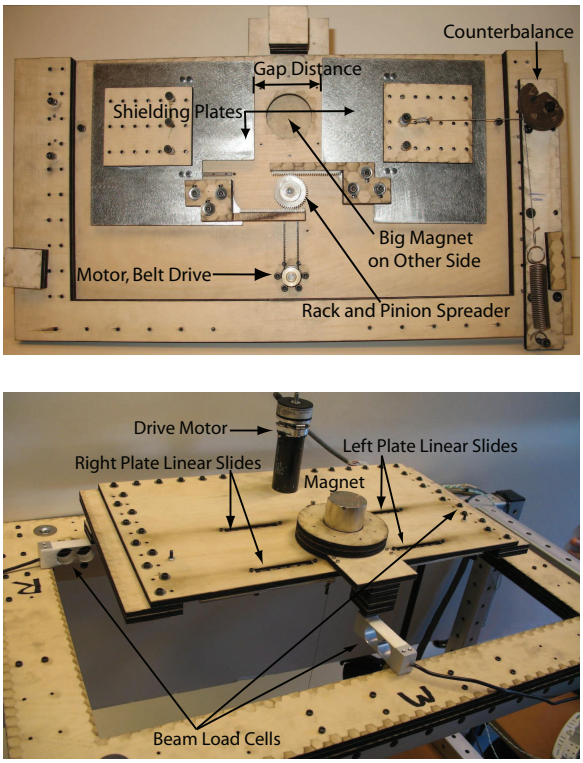

Fig. 5. Force regulation mechanism and weighing system.

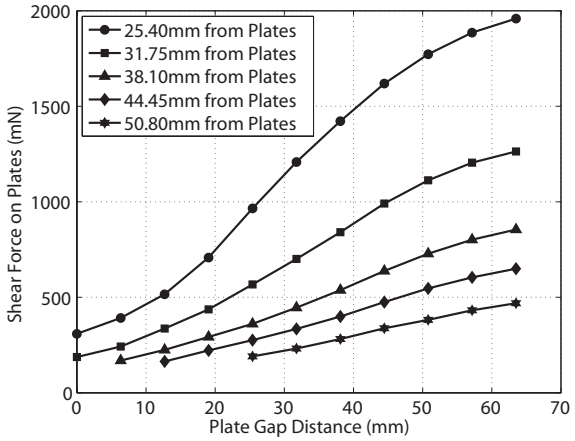

Fig. 6. Force on the small magnet vs. plate gap distance for double-stacked shielding plates. Each curve represents a different fixed distance between the small magnet and the shielding plates, or ultimately the controlling magnet.

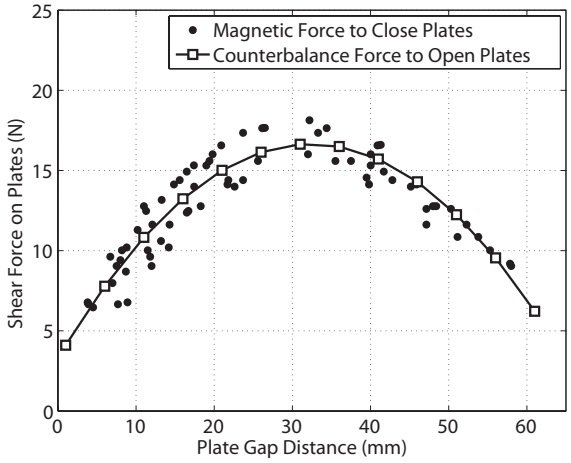

Fig. 7. Shear force and design of counterbalance system for double-stacked shielding plates. The fitted curve represents the designed counterbalance force profile to best cancel the experimentally determined shear force.

that could support the operating loads were massive and posed a much larger risk of magnetic interaction.

B. Parabolic Counterbalance

To achieve higher bandwidth in our system, we wanted to avoid using a gearhead on the motor. However, the substantial magnetic shear forces on the plates proved excessive for a reasonably-sized motor. One solution is to use springs attached to the plates to cancel the magnetic shear force, but the force profile of a linear spring does not correspond well with the parabolic profile of the shear force. Accordingly, we used a counterbalance with a special pulley profile to provide a parabolic force profile to balance the magnetic force on the plates, as shown in Figure 7.

The parabolic counterbalance system uses a cable-driven dual capstan to convert the linear force profile of an extension spring to a parabolic force profile that will cancel the shear force of the magnet on the shielding plates. The dual capstan consists of a spiral capstan and a constant-diameter capstan that are connected rigidly and mounted on a ball-bearing pivot. One end of the extension spring is fixed to ground, and the free end of the spring attaches to a steel cable that wraps around the spiral capstan. A second cable wraps around the constant-diameter capstan and attaches to one of the shielding plates. Any movement to open the plates results in further shortening of the extension spring and a reduction in spring force. However, opening the plates also rotates the spiral pulley such that the tangent radius at which the spring force is applied increases. By controlling how quickly the tangent radius increases with rotation, we can choose to either decrease or increase the torque at any given position that is generated by the always-decreasing spring force. Figure 8 shows a free-body diagram of the dual capstan.

The linear position x of the shielding plate, corresponding to a plate gap distance of $2x$, results in a rotation λ of the constant-diameter pulley of radius R_{const} and the entire dual capstan,

$$x = R_{const}\lambda. \tag{2}$$

This relationship allows us to parameterize the desired parabolic counterbalance force profile, shown in Figure 7, as a function of rotation angle, $F_{bal}(\lambda)$.

The torques on the pulleys $\tau_{const}(\lambda)$ and $\tau_{spiral}(\lambda)$ are defined as:

$$\tau_{const}(\lambda) = F_{bal}(\lambda)R_{const}, \tag{3}$$

$$\tau_{spiral}(\lambda) = F_{spring}(\lambda)R_{spiral}(\lambda). \tag{4}$$

Since the spiral and constant-diameter pulleys are rigidly

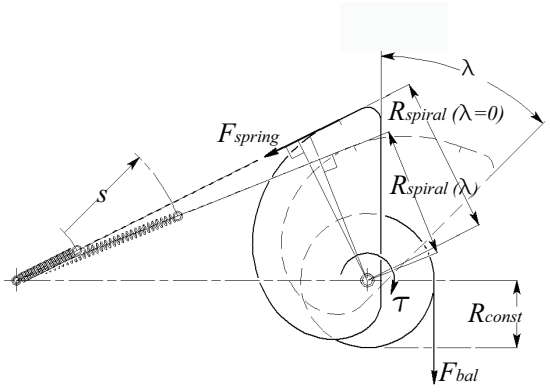

Fig. 8. Free-body diagram of counterbalance system.

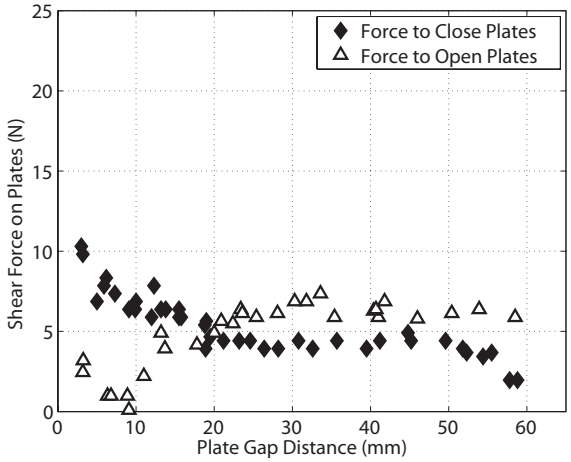

Fig. 9. Residual force required to move the plates from rest after the counterbalance is applied. This is the result of model inaccuracy and stiction in the counterbalance system.

connected, these torques on the pulleys are equal and opposite, leading to a relationship between F_{bal} and F_{spring}. By appropriately varying the tangent radius R_{spiral} of the spiral pulley as a function of rotation angle λ, the dual capstan can convert the linear force profile of the spring F_{spring} to a parabolic force profile F_{bal}. The goal is to find an appropriate $R_{spiral}(\lambda)$ force for this conversion:

$$R_{spiral}(\lambda) = \frac{F_{bal}(\lambda)R_{const}}{F_{spring}(\lambda)}. \quad (5)$$

This can be performed by solving for local tangent radii as we rotate the dual capstan incrementally. Begin by considering a rotation of $\Delta\lambda$ from an angle of λ_{i-1} to λ_i. Assume that we have already solved for all previous radii $R_{spiral}(\lambda_j)$, j < i and wish to solve for the next local tangent radius R_{spiral} (λ_i). The total compression $S(\lambda_{i-1})$ of the spring from its initial (S = 0, λ = 0) length is given by

$$S(\lambda_{i-1}) = \sum_{k=0}^{i-1} R_{spiral}(\lambda_k)\Delta\lambda = \Delta\lambda \sum_{k=0}^{i-1} R_{spiral}(\lambda_k). \quad (6)$$

For an extension spring with a stiffness of K and initial tension $F_{spring0}$, that compression $S(\lambda_{i-1})$ yields a new tension $F_{spring}(\lambda_i)$ of

$$F_{spring}(\lambda_i) = KS(\lambda_{i-1}) + F_{spring0}. \quad (7)$$

The new tangent radius R_{spiral} (λ_i) is then calculated as

$$R_{spiral}(\lambda_i) = \frac{F_{bal}(\lambda_i)R_{const}}{F_{spring}(\lambda_i)}. \quad (8)$$

It should be noted that not all values of K, R_{const}, and $F_{spring0}$ yield real solutions, so some iteration is required.

Figure 9 shows the experimentally measured residual shear force on the shielding plates after incorporating the counterbalance. Although the counterbalance cancelled much of the magnetic shear force, including reducing the peak force by a factor of three, model inaccuracies and stiction resulted in an average residual force required to move the plates of 6N.

C. Weighing System

For our closed-loop force control, we measured the force on the small magnet indirectly by measuring the equal and opposite force on the large magnet. Measuring the force on the large magnet externally removes the need for placing additional instrumentation on the small magnet. The external force measurement system consisted of three fixed beam load cells that supported the weight of the entire force control system. Since the small magnet has negligible attraction to the shielding plates themselves, weighing the entire control system measures the pull of the small magnet on the large magnet and visa versa. This method is in contrast to placing the force sensor directly on the large magnet, wherein the sensor would also measure the attractive force of the large magnet to the shielding plates and require a look-up table to parse out only the force from the small magnet.

IV. CONTROL

To control the force exerted by the large magnet on the small magnet, we set up a control system based on successive loop closure. The general idea is that inner and outer loops in the block diagram are identified and separated by their respective bandwidths. This requires the inner loop to have faster dynamics than the outer loop to avoid instabilities. For our system, as shown in Figure 10, the inner loop is designed for angular position control of the DC motor, which generates the spreading of the shielding plates. The inner loop tracks a desired angle $\theta_{desired}$, and the corresponding output is the actual angle θ_{actual} as measured by an optical encoder. We use a simple PD-controller for K_{inner}. The inner loop was tuned experimentally by commanding an arbitrary angle $\theta_{desired}$ and increasing the proportional gain until the motor started to vibrate. We then selected a proportional gain that was slightly lower than the instability point. To tune the derivative gain we applied step inputs on $\theta_{desired}$ and adjusted the gain until an acceptable response was found.

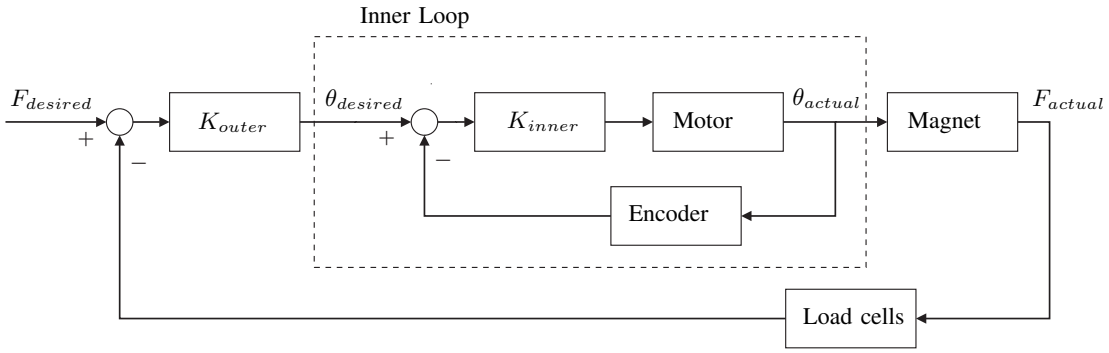

Fig. 10. Block diagram for control using successive loop closure. K_{outer} is a PID controller. K_{inner} is a PD controller.

The outer loop of our system is designed for force control on the small magnet. The outer loop tracks a desired force input $F_{desired}$, and the corresponding output is the actual force F_{actual} as measured by the load cells. Although a simple PD-control law would be desirable, this cannot be used due to the inherent fighting between the inner and outer loops. That is, if the outer loop is trying to set the error term ($F_{actual} - F_{desired}$) to zero, this results in a commanded angle of zero as well (when the commanded angle is most likely non-zero). To avoid this fighting, we add an integral term and use PID-control for K_{outer}. This ensures that the force error term is driven to zero, while the commanded angle is kept at the correct non-zero value. As before, the outer loop was tuned experimentally to find an optimal response.

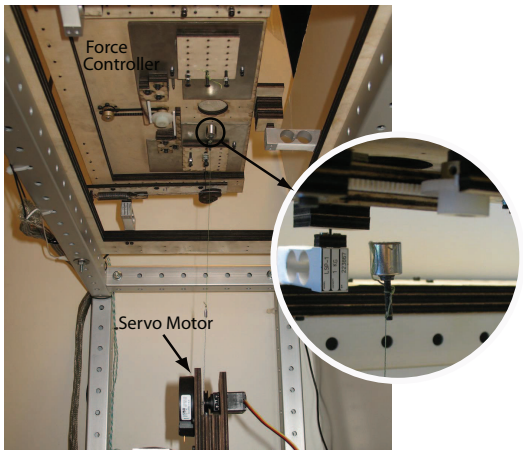

Fig. 11. Force regulation experimental setup. The inset shows the small magnet suspended below the force control system.

V. FORCE-REGULATION EXPERIMENT

One possible application of our force regulation system is to keep a constant force on a magnetic catheter tip as it moves inside of the body at varying distances from the external, controlling magnet. This scenario requires force regulation because the magnetic catheter tip will experience higher forces as it moves closer to the external magnet and lower forces as it moves further away. By regulating a constant force regardless of the catheter tip's trajectory, we could provide more consistent, controlled contact between the catheter tip and tissues for a variety of procedures. Towards this end, we have designed an experiment to test the force regulation capabilities of our system.

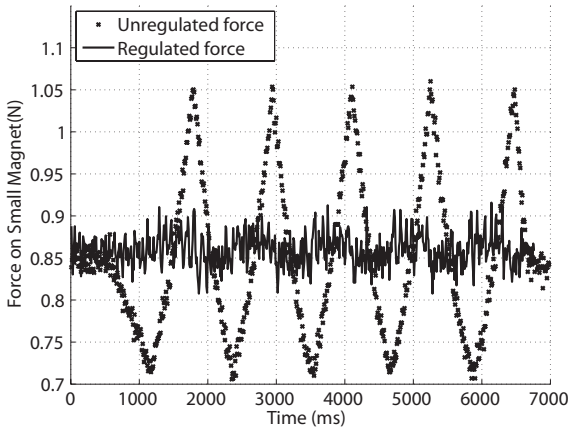

Fig. 12. Unregulated and regulated force on the moving small magnet with a saw-tooth trajectory. Note that the maximum force corresponds to minimum distance between the magnets. Force regulation occurred about the force level encountered at the centerline of the trajectory.

Our experimental setup consists of the small magnet suspended from a string below the force controller, as shown in Figure 11. The string wraps around a capstan that is driven by a servo motor to provide control over the separation distance between the small magnet and the force controller, or ultimately the large magnet. For simplicity, we chose to move the small magnet in a saw-tooth trajectory that is centered at 38.1mm from the shielding plates and has an amplitude of $\pm$7.25mm. The period is roughly one second. We selected the desired regulated force to be the force felt at the centerline of the trajectory. Figure 12 shows both the unregulated and regulated forces on the small magnet as it moves through its trajectory. The force regulation provides a roughly constant, correctly-centered force profile that reduces the amplitude of the profile about the desired force by at least 82 percent.

VI. CONCLUSION

In this paper we presented a proof-of-concept system for closed-loop force control of a permanent magnet using actuated shielding materials. We first demonstrated the ability of high permeability materials to redirect magnet lines of flux and compared this to FEA simulations. We then discussed the mechanical design of our device and counterbalance system as well as a control strategy based on successive loop closure. Finally, we presented experimental results for successful contant-force control of a small, moving magnet at forces and distances that are medically relevant.

Much work remains towards making our system clinically viable for control of medical devices such as robotic catheters. We plan to perform more extensive FEA simulations so that we can design our system's force reduction profile in software before construction. Practical issues that need to be addressed include operation of the system at different angles and workspace extension. Operating the device at different angles would require using a multidimensional force sensor and measuring the orientation of the device with respect to gravity to parse out the pull of the small magnet from the weight of the device. Extending the workspace could involve using pushpull pairs of magnets and/or using larger magnets that could potentially be focused with additional shielding techniques.

Another possible area of future work is sensing the position of the small magnet within the body. Figure 6 demonstrates that positioning the small magnet at different distances from the shielding plates, or ultimately the controlling magnet, produces a family of force-gap curves with each distinct curve corresponding to a distinct distance between the magnets. It is theoretically possible that we could use this family of curves to estimate the distance between the two magnets simply by measuring the force and gap distance at a particular time and checking which curve contains that force, gap combination. This could provide a rough means of recreating the trajectory of the small magnet.

VII. ACKNOWLEDGMENTS

R. Brewer was supported in part by an ASEE NDSEG Fellowship, and K. Loewke was supported in part by a NSF Graduate Research Fellowship. The authors thank Dr. Gunter Niemeyer for his advice regarding the control system and Dok Won Lee for performing the magnetic FEA simulation.

REFERENCES

[1] Ansoft corp. Maxwell 3D, http://www.ansoft.com/.
[2] Given imaging website. http://www.givenimaging.com/.
[3] Hansen medical, inc. website. http://www.hansenmedical.com/.
[4] National electronic alloys. Hyperco Alloy 50 Technical Sheet, http://www.nealloys.com/.
[5] Stereotaxis, inc. website. http://www.stereotaxis.com/.
[6] Vdm nickel-technologie ag. Magnifier 7904 Material Data Sheet, http://www.thyssenkrupp-steel.com/de/.
[7] Vdm nickel-technologie ag. Magnifier 50 Material Data Sheet, http://www.thyssenkrupp-steel.com/de/.
[8] A. Al-Ahmad. Utilizing robotic catheter control technology for ep procedures. *EP Lab Digest*, 7(8):20–22, 2007.
[9] D. Camarillo, T. Krummel, and K. Salisbury. Robotic technology in surgery: past, present, and future. *American Journal of Surgery*, 188(4A):2S–15S, 2004.
[10] M. Faddis, W. Blume, J. Finney, A. Hall, J. Rauch, J. Sell, K. Bae, M. Talcott, and B. Lindsay. Novel, magnetically guided catheter for endocardial mapping and radiofrequency catheter ablation. *Circulation*, 106(23):2980–2985, 2002.
[11] G. Guthart and K. Salisbury. The intuitive telesurgery system: overview andapplication. *Proceedings of the International Conference on Robotics and Automation*, pages 618–621, April 2000.
[12] R. C. O'Handley. *Modern Magnetic Materials: Principles and Applications*, page 25. John Wiley and Sons, 200.
[13] R. Satava. Emerging technologies for surgery in the 21st century. *Archives of Surgery*, 134(11):1197–1202, 1999.
[14] M. Schiemann, R. Killmann, M. Kleen, N. Abolmaali, J. Finney, and T. Vogl. Vascular guide wire navigation with a magnetic guidance system: Experimental results in a phantom. *Radiology*, 232(2):475–481, 2004.
[15] G. Schwarze. Advanced electrical materials and components development - an update. *Proceedings of the 3rd International Energy Conversion Engineering Conference*, pages 15–18, August 2005.
[16] R. Taylor. Robots as surgical assistants: Where we are, wither we are tending, and how to get there. *Proc. AIME*, pages 3–11, 1997.
[17] H. Tillander. Magnetic guidance of a catheter with articulated steel tip. *Beta Radiology*, 35:62–61, 1951.
[18] I. Tunay. Modeling magnetic catheters in external fields. *Proceedings of the International Conference of the Engineering in Medicine and Biology Society*, pages 2006–2009, September 2004.
[19] K. Xu and N. Simaan. Actuation compensation for flexible surgical snake-like robots with redundant remote actuation. *Proceedings of the International Conference on Robotics and Automation*, pages 4148–4154, May 2006.